PAPER

Check for updates

Metal-free cysteamine-functionalized graphene alleviates mutual interferences in heavy metal electrochemical detection†

Qiuyue Yang, [ID] [a,b] Emily P. Nguyen,[a] David Panáček,[a,c] Veronika Šedajová, [ID] [c] Vítězslav Hrubý,[c,d] Giulio Rosati,[a] Cecilia de Carvalho Castro Silva, [ID] [a,e] Aristides Bakandritsos, [ID] [c,f] Michal Otyepka [ID] [c,g] and Arben Merkoçi [ID] ⋆[a,h]

Heavy metal pollutants are of great concern to environmental monitoring due to their potent toxicity. Electrochemical detection, one of the main techniques, is hindered by the mutual interferences of various heavy metal ions in practical use. In particular, the sensitivity of carbon electrodes to Cd^{2+} ions (one of the most toxic heavy metals) is often overshadowed by some heavy metals (*e.g.* Pb^{2+} and Cu^{2+}). To mitigate interference, metallic particles/films (*e.g.* Hg, Au, Bi, and Sn) typically need to be embedded in the carbon electrodes. However, these additional metallic materials may face issues of secondary pollution and unsustainability. In this study, a metal-free and sustainable nanomaterial, namely cysteamine covalently functionalized graphene (GSH), was found to lead to a 6-fold boost in the Cd^{2+} sensitivity of the screen-printed carbon electrode (SPCE), while the sensitivities to Pb^{2+} and Cu^{2+} were not influenced in simultaneous detection. The selective enhancement could be attributed to the grafted thiols on GSH sheets with good affinity to Cd^{2+} ions based on Pearson's hard and soft acid and base principle. More intriguingly, the GSH-modified SPCE (GSH-SPCE) featured high reusability with extended cycling times (23 times), surpassing the state-of-art SPCEs modified by non-covalently functionalized graphene derivatives. Last, the GSH-SPCE was validated in tap water.

aNanobioelectronics and Biosensors Group, Catalan Institute of Nanoscience and Nanotechnology (ICN2), CSIC, Campus UAB, Bellaterra, Barcelona 08193, Spain. E-mail: arben.merkoci@icn2.cat

bDepartment of Materials Science, Universitat Autònoma de Barcelona, Campus de la UAB, Plaça Cívica, 08193 Bellaterra, Barcelona, Spain

cRegional Centre of Advanced Technologies and Materials, Czech Advanced Technology and Research Institute (CATRIN), Palacký University Olomouc, Šlechtitelů 27, 783 71 Olomouc, Czech Republic

dDepartment of Physical Chemistry, Faculty of Science, Palacký University Olomouc, 17. listopadu 12, 771 46 Olomouc, Czech Republic

eMackGraphe-Mackenzie Institute for Research in Graphene and Nanotechnologies, Mackenzie Presbyterian University, Consolação Street 930, 01302-907 São Paulo, Brazil

fNanotechnology Centre, Centre of Energy and Environmental Technologies, VŠB–Technical University of Ostrava, 17. listopadu 2172/15, 708 00 Ostrava-Poruba, Czech Republic

gIT4Innovations, VSB–Technical University of Ostrava, 17. listopadu 2172/15, 708 00 Ostrava-Poruba, Czech Republic

hInstitució Catalana de Recerca i Estudis Avançats, Pg. Lluís Companys, 23, Barcelona 08010, Spain

†Electronic supplementary information (ESI) available. See DOI: https://doi.org/10.1039/d2gc02978b

1. Introduction

Heavy metal (HM) pollutants influence important access to clean water due to the risks of toxicity, bioaccumulation, biomagnification, and environmental persistence.[1,2] On the Environmental Quality Standards Directive List, As, Cd, Cr, Cu, Fe, Ni, Pb, Hg, and Zn are underlined as key substances for evaluating water quality.[3] Although some HM elements (*e.g.* Cu) are necessary for human health, ingestion of these HMs is harmful at high concentrations[4,5] while other HMs, such as Cd and Pb are harmful even at the ppb range to the ecosystem and bioaccumulate in the human body *via* the foods we eat.[5] Therefore, HM analysis within primary food sources (*e.g.* drinking/tap water) is important.

Given their simplicity and low cost, electrochemical techniques are ideal for HM ion analysis. Amongst these, square-wave anodic stripping voltammetry (SWASV) is favourable due to its resilience to dissolved oxygen in real samples.[6,7] When determined by SWASV, HM cations are first reduced on the working electrode surface at a negative potential over a certain period of time (in minutes); then the potential is increased to a positive value with a ramp upon which a square waveform is

superimposed; moreover, reduced HMs are oxidized to the corresponding cations, generating discrete anodic current peaks. Consequently, the corresponding peak potential allows the identification of HM species, and the peak intensity or area is proportional to the HM concentration.

In the field of HM detection by SWASV, carbon electrodes have gradually replaced the hanging mercury drop electrode (HMDE) due to the toxicity of Hg.[8] However, bare carbon electrodes suffer from mutual interference due to the lack of an effective working surface in comparison to HMDEs. This could induce ion competition and intermetallic compounds in the deposition step, which are generally regarded as two major reasons for mutual interference.[8–10] Mutual interference often results in unexpected outcomes, including a drop in sensitivity, shifting of the peak potential, peak splitting, and peak overlapping.[11] In particular, the sensitivity to Cd^{2+} is diminished by the presence of Pb^{2+} or Pb^{2+} and Cu^{2+} when determined using screen-printed carbon electrodes (SPCEs),[12,13] glassy carbon electrodes (GCE),[14] or boron-doped diamond electrodes (BDDs).[15] Mutual interference makes the detection of Cd^{2+} incredibly challenging with the existence of Pb^{2+} and Cu^{2+} ions, which commonly appear in many waters. Solving this issue is more daunting for SPCEs as their rough surface tends to induce mutual interference compared to other carbon electrodes.

The most typical alleviating strategy is to deposit metallic substances (*e.g.* Bi,[16] Hg,[17] Sn,[18] and Au[19]) on carbon electrodes to mimic the HMDE.[20] Despite the effectiveness of this strategy, most of these metals are scarce in the earth's crust, which renders them unsustainable, together with recycling issues, while the mining and smelting may cause secondary pollution to the environment.[21] Amongst them, on account of its moderate cost and low toxicity, Bi, generally regarded as a "green metal", is one of the most favoured ones,[22] although recently the greenness of some Bi complexes has been doubted.[23] Besides, owing to the working principle of metallic electrodes forming alloys with HM ions in the deposition step, the electrodes tend to lose their component substances in the formed alloys during stripping, thus resulting in only being able to be reused a relatively few times (~10 times),[24–26] which could limit their application with the developments of *in situ* and automatic sensing tools used for water quality control in large lakes and rivers recently.[27] Furthermore, emerging 2D materials (*e.g.* Ti_3C_2) and porous materials (*e.g.* ZIF-8) are employed to enhance Cd^{2+} sensitivity under mutual interference.[28,29] In a bigger scope, general mutual interference can be reduced by the use of other nano-structured metal compounds.[30–32] However, the synthesis of these materials relies on reactions involving metal salts as precursors, which induces similar problems. Therefore, green and stable nanomaterials are highly demanded in order to alleviate mutual interference issues.

Fortunately, bio- and carbon-based nanomaterials rich in N, S, and O also appear to be able to address the issue due to their good affinity towards specific HM ions. Choi *et al.* utilized graphene oxide (GO)-doped diaminoterthiophene to modify the SPCE and reported an enhanced sensitivity of the SPCE to Cd^{2+} with the presence of Hg^{2+}, Cu^{2+}, and Pb^{2+}.[33] However, the disposal device could not operate under continuous measurement, which is the final hurdle to overcome. Hence, reusable biofunctionalized nanomaterials are highly sought.

Graphene as a 2D nanomaterial is a good host for biofunctionalization due to the large basal area.[34] The functionalization of graphene is primarily divided into non-covalent and covalent functionalization.[35] Non-covalent functionalization takes advantage of the π-interactions, hydrogen bonding, van der Waals force, *etc.* between graphene and functionalization agents, while covalent functionalization creates a more robust chemical bond between the two. Thus, covalent moieties are extremely stable on the graphene surface.[36] Accordingly, covalently biofunctionalized graphene derivatives seem promising to address mutual interferences while maintaining high stability and reusability. Nevertheless, the most commonly used precursors, GO and reduced graphene oxide (rGO), pose challenges to homogeneous and manageable functionalization due to their non-uniform distribution of oxidized groups.[37,38]

As such, a new methodology for functionalizing graphene covalently has been investigated,[39] in which fluorographene (FG) is used as a precursor with uniformly distributed fluorine. Controllable graphene chemistry can be accessed through the nucleophilic substitution reaction on the FG and the simultaneous defluorination.[40] For example, it was reported that carboxylic groups could be uniformly and covalently functionalized on graphene sheets (and to form graphene acid, GA) *via* the mild hydrolysis of cyanographene, which is a practically fluorine-free graphene derivative with covalently bonded nitrile groups synthesized from FG.[41] The carboxyl groups on the GA then behave as versatile anchoring sites to conjugate with many biomolecules. These formed derivatives have been utilized in versatile applications, like energy storage,[42] sensing,[43] and catalysis.[44] More excitingly, since organic amines commonly appear in biomaterials and are known to be good nucleophiles,[45] they can react with FG, affording materials with molecules grafted on the graphene backbone directly *via* the covalent bonds of amino groups with the graphene surface. This covalent functionalization strategy can open the way to facile and flexible functionalization with various biomolecules.

This study is, to the best of our knowledge, the first to report the synthesis of a cysteamine-functionalized graphene (GSH) by this covalent functionalization strategy and then its modification on the screen-printed carbon electrode (SPCE), with an aim to solve mutual interferences without requiring any metallic additives. By leveraging the binding proclivity of thiol residues on the GSH towards the softer Cd^{2+} ions based on Pearson's hard and soft acid and base principle (HSAB), the GSH was expected to enhance the sensitivity of the SPCE to Cd^{2+}. Hence, the role of the GSH was examined for simultaneous HM ions (*i.e.* Cd^{2+}, Pb^{2+}, and Cu^{2+}) detection in a flow injection system designed for *in situ* and automatic measurements (Fig. 1a and Fig. S1†) based on SWASV (Fig. 1b).
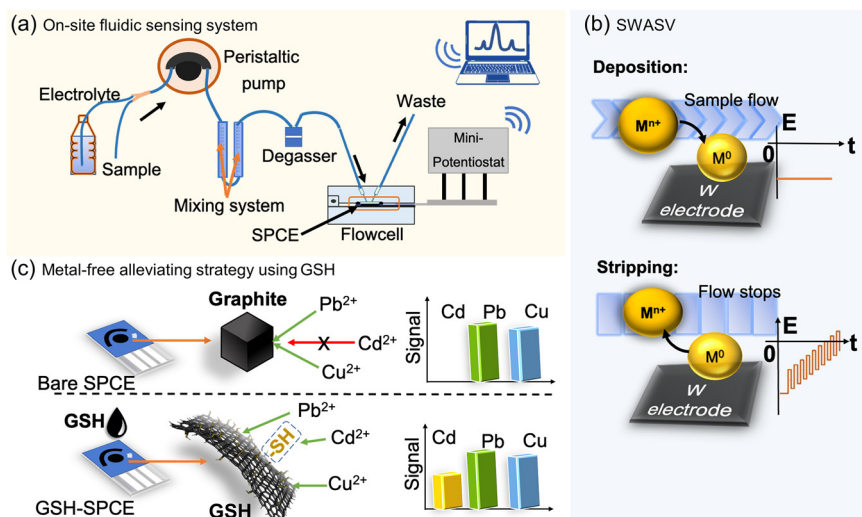
Fig. 1 Schematic illustration of the working principle in our study. Schematic illustration of the (a) flow injection system used for *in situ* HM detection, allowing the sample and supporting electrolyte to mix automatically, and to flow through the surface of the SPCE in the deposition step and to stop in the stripping step during SWAVS; (b) two main two of SWASV: the deposition and stripping steps; and (c) use of GSH for Cd^{2+}-sensing enhancement compared with a bare SPCE by the functionalized cysteamine moieties and graphene-like 2D structure.

Besides, the GSH was benchmarked against other graphene derivatives functionalized with other groups, verifying its superior sensitivity to Cd^{2+} (Fig. 1c). Furthermore, continuous cycling measurements were tested by using the GSH-SPCE with the expectation of a greater sensing reusability due to the covalent functionalization of the thiol groups on the graphene surface. Last, the GSH-SPCE was used to for detection in real samples.

2. Experimental section

2.1 Reagents and equipment

The SPCEs were fabricated with a DEK248 printer machine (DEK, Weymouth, UK). The Ag/AgCl ink was Loctite EDAG AV458 (Henkel). The carbon paste was C2030519P4 CARBON SENSOR PASTE (267508), the Ag ink was C2180423D2 SILVER PASTE 349288, and the insulating ink was D2070423P5 DIELECT PASTE GREY (all from Sun Chemical). Deionized water (18.2 MΩ·cm at 25 °C, Milli-Q) was used throughout for all the experiments. The 37% hydrochloric acid was 320331-2.5L from Sigma. Standard HM solutions (Cd^{2+}, Cu^{2+}, and Pb^{2+} 1000 ppm, Sigma) were all AAS grade. GO water solution (N002-PS-1.0) was acquired from Angstron Materials (Dayton, OH, USA).

The concentration of graphene supernatants was estimated by UV–VIS spectrophotometry (UV-1900, Shimadzu). The morphology of the material was characterized by SEM analysis with a Hitachi SU6600 instrument with an accelerating voltage of 5 kV, and by TEM analysis with a JEM 2010 TEM instrument (Jeol, Japan). The FTIR characterization was operated on an iS5 FTIR spectrometer (Thermo Nicolet), equipped with a Smart Orbit ATR accessory with ZnSe crystal. FTIR spectra were

smoothed and baseline corrected for better clarity. GSH was characterized by the XPS technique (PHI VersaProbe II physical electronics spectrometer) using an Al Kα source (15 kV, 50 W), on a MultiPak system (Ulvac-PHI, Inc.). A software package was used to evaluate the obtained data. Raman analysis was operated on a DXR Raman microscope using a diode laser's 633 nm excitation line. The spiked tap water was analysed in a 7500ce inductively coupled plasma mass spectrometry (ICP-MS) instrument (Agilent).

2.2 Synthesis of the GSH

First, 2 g of graphite fluoride (61 < at% F, polymer, Sigma-Aldrich) was dispersed in 120 ml of DMF (for peptide synthesis, Merck), followed by continuous stirring for 72 h at room temperature. Then, the dispersion was sonicated in an ultrasonication bath for 4 h (<60 °C) and was kept stirring for another 24 h at room temperature. Last, 10.2 g K_2CO_3 (Penta) and 5 g cysteamine (Sigma-Aldrich) were added to the dispersion and left stirring under heating at 130 °C for 24 h in an oil bath in the hood with a condenser for reflux.

When cooling down, the formed product was centrifuged (20 000 rcf per 10 min) and washed with DMF (2×), hot DMF (1×), acetone (2×), hot acetone (1×), ethanol (3×), distilled water (2×), and hot distilled water (1×).

To decompose the possible unwanted disulfide bonds in the GSH, the whole amount of the synthesized material was mixed with 420 μL of 2-mercaptoethanol (Carl Roth; ~2× molar ratio of –SH groups considered as 20% F.D.), and left shaking for 30 min. Then, the material was additionally washed with ethanol (1×), acidified distilled water (2×), and distilled water (1×) using centrifugation (20 000 rcf per 10 min) and purified by being placed into the dialysis membrane (cut-off 14 kDa) in a container of distilled water (5L) that was

changed every day until the dispersion containing the material reached a conductivity <100 μS cm^{-1}.

2.3 Preparation of GSH-SPCEs

SPCEs were fabricated the same as reported in our previous study.[27] For better quality control, all the SPCEs were cleaned in 0.05 M HCl and deionized water, and then pre-tested by SWASV. According to the obtained stripping curves (charge *vs.* potential), the SPCEs were selected only within the charge range of 2–4 mC. Additional cyclic voltammetry (10 scans) was performed with the selected SPCEs in 0.05 M HCl for further cleaning.

A suspension of the graphene derivatives (GSH, GA, and GO, 1 mg ml^{-1}) was sonicated in a bath for 30 min at room temperature and then centrifuged at 9000 rpm for 1 min. Next, 5 μL of the GSH supernatant (~0.016 mg ml^{-1}) was pipetted onto the working electrode of a cleaned SPCE and dried at 37 °C in an oven. Depending on the total modified volume (10, 15, and 20 μL), the drop-casting procedure was repeated several times in 5 μL increments. Other graphene derivatives (GA and GO) supernatants followed the same approach, except their concentrations were adjusted equal to that of the GSH supernatant. All the supernatant concentrations were estimated by UV–Vis using the Beer–Lambert equation, whereby the molar absorptivity was 3463 ml mg^{-1} m^{-1}.[46] The GO-SPCE was reduced (to rGO-SPCE) in the cyclic voltammetry tests (CV, 10 scans) between −1.1 and 0 V, then by chronopotentiometry at −1.1 V for 200 s.

2.4 HM detection by SPCEs

HM analysis was conducted in the fluidic injection system shown in Fig. 1 and as per our previous study.[27] Fig. S1† describes the working principle of this system in detail. The frequency of the square waves was 25 Hz with an amplitude of 30 mV and a potential step of 6 mV. The equilibrium time was 20 s.

2.5 Data analysis

The integral area under each peak (A) in voltammograms was used as the sensing signal instead of the peak current due to peak splitting, where A is the integral of the splitting peak area (two subpeaks in total), which was calculated using the software PStrace 5.8 (PalmSens). The LOD was estimated based on the International Conference on Harmonization's Q2 Validation of Analytical Procedures by:[47]

$$LOD = 3\sigma/S$$

where σ and S are the intercept standard error and the slope of the fitted calibration line, respectively, obtained using Origin 2018 software. The sensitivity (S) is defined as the calibration slope. Repeatability is defined as the relative standard deviation (RSD) of the sensing signals from continuous measurements. Reproducibility is the RSD of the sensitivities collected from different SPCEs in one batch. The *t*-test used was the 2-tailed Student's *t*-test with heteroscedasticity conducted in

Microsoft Excel. Recovery was determined as the tested concentration divided by the spiked concentration.[48]

3. Results and discussion

3.1. Synthesis and characterizations of the GSH

The GSH was synthesized through the substitution of F on fluorographene (FG) by the amino groups (–NH$_2$) on cysteamine (Fig. 2a). The defluorination and functionalization occurred simultaneously owing to the nucleophilic substitution.[49] To secure the deprotonation of the amino groups (and thus their maximum nucleophilicity), potassium carbonate (K$_2$CO$_3$) was used as a base to scavenge protons from the system, preventing the formation of the by-product, hydrogen fluoride (HF), during the synthesis. Additionally, K$_2$CO$_3$ boosted the surface area of the resulting material thanks to the release and expansion of carbon dioxide.[50]

The SEM and TEM images in Fig. 2(b–d) demonstrate typical 2D sheets of functionalized graphene with a wrinkled morphology.

The FTIR results showed that the GSH was a fluorine-free graphene-based material, due to the absence of a sharp feature at 1200 cm^{-1} originating from C–F bond vibration, while this feature was apparent in the pristine graphite fluoride (GF) material (Fig. 2e). The development of sp^2 regions was evident from the strong C=C band at 1550 cm^{-1}. The broad feature in the region between 1300 and 1050 cm^{-1} is common for many graphene-based materials, representing a large group of vibration modes whose bands are mutually indistinguishable. The largest part of the features represented graphene's in-plane C–C bond stretching,[41] while C–S,[51,52] C–N,[53] and C–O[54] species of the immobilized cysteamine molecules and oxygen contamination may also have contributed to its intensity and broadness. Last, among this broadband, two sharp maxima at 1123 and 1023 cm^{-1} were distinguishable. The shoulder at 1450 cm^{-1} was assigned to C–H bending, which was the only proof of the presence of C–H bonds, since the C–H stretching band at 2900 cm^{-1} was barely observable.[50] Last, a broad feature manifested between 3050 and 3500 cm^{-1} was assigned to O–H and N–H stretching vibrations.[50]

The elemental composition from the XPS analysis (Fig. 2f) showed that the GSH was nearly fluorine-free (1.2 at%) containing C, N, and S atoms, complying with the results from FTIR. The minimal oxygen content could either originate from the DMF molecules reacting with the GF during functionalization,[41] or from adventitious contamination from the environment. The functionalization degree (F.D.) was estimated to be 3.5% based on the S/C ratio.[41] In the C 1s region of the XPS spectrum (Fig. 2g), carbon atoms were found mainly in the sp^2 hybridization state, further proving the graphene-like nature of the material observed from the FTIR results, while the other components found at higher binding energies corresponded to sp^3-hybridized carbon atoms, mostly from the alkyl chains of cysteamine functionalities and the carbon bonded to sulfur, nitrogen, and oxygen atoms, and to
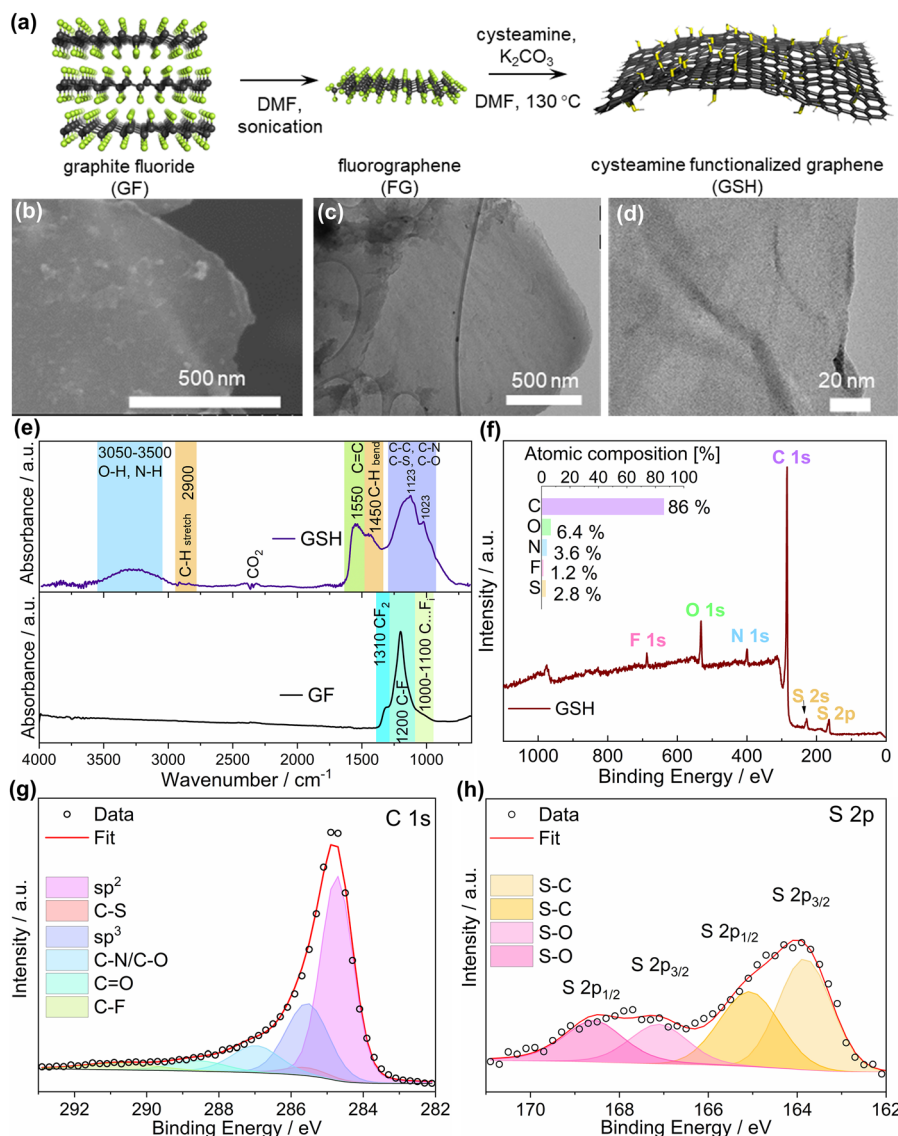
Fig. 2 Characterizations of the GSH. (a) Schematic illustration of the synthesis. (b) Scanning electron microscopy (SEM), (c) transmission electron microscopy (TEM), and (d) magnified TEM images of the GSH sheet. (e) Fourier-transform infrared spectroscopy (FTIR) spectra of the GSH and graphite fluoride (GF). (f) X-Ray photoelectron spectroscopy (XPS) survey spectrum and element composition analysis. High-resolution XPS spectra for (g) C 1s and (h) S 2p.

residual fluorine with primarily overlapping binding energy values.

In the deconvolution of the S 2p envelope, the sulfur atoms of GSH were mostly bonded to carbon atoms, as indicated by the component at 163.9 eV for S $2p_{3/2}$ which further proved the successful functionalization, although some sulfur atoms were also bonded to oxygen atoms, as evident from the presence of additional components at higher binding energy values (Fig. 2h).[55]

A broad D band and rather high I_D/I_G ratio (1.26) in the Raman spectrum (Fig. S2†) indicated that the GSH contained a high number of defects within the graphene backbone. This phenomenon should stem mainly from the sp³ carbon atoms, signifying the successful bonding between cysteamine func-

tionalities and the graphene sheet, and thus, reflecting the high F.D. of the material. Moreover, the sharp G-band showed that the GSH had developed a network of sp² carbon, denoting a high degree of reductive defluorination, which also accorded with the C 1s spectrum in the XPS results, in which the carbon sp² hybridized atoms constituted a dominant fraction of the GSH (Fig. 2g).

Overall, the characterization results allowed concluding that the reaction of FG with cysteamine afforded a graphene-like material functionalized with thiol groups. This was thanks to the covalent bond between the cysteamine molecules *via* their amino groups and the graphene sheet. However, it is important to note that to further comply with green chemistry principles, the replacement of DMF in syntheses with more

benign solvents will be required due to health-related concerns. Our recent work demonstrated the possibility to achieve this goal, showing the functionalization of fluorographene (in a different reaction), which took place similarly effectively both in DMF and in acetonitrile.[56] Thus, it is anticipated that the reaction of fluorographene with cysteamine could be also furnished in acetonitrile, which will be the subject of a follow-up work related to a different application.

3.2 Sensing performance of the GSH-SPCE compared to the bare SPCE

3.2.1 Fabrication, optimization, and sensing performance of the GSH-SPCE in individual HM solutions. The GSH-SPCE was prepared by drop casting, in which the supernatant of GSH ($\sim$0.016 mg ml^{-1}) was pipetted on the working electrode of a cleaned bare SPCE. After the supernatant had completely evaporated, the procedure was repeated once more to achieve the best modification.

All the following experiments were operated under the optimized situation, *i.e.* HCl as a supporting electrolyte at 0.05 M, pipetted GSH supernatant volume of 10 μL, and deposition potential of −1.0 V with a flowrate of 3 ml min^{-1} and flowtime of 200 s, as shown in Fig. S3–S5 and Table S1.†

Bare SPCE and GSH-SPCE were first employed to detect Cd^{2+}, Pb^{2+}, and Cu^{2+} individually with different concentrations to determine their sensitivities (S, denoted as the slope of the calibration line). Compared to the bare SPCE, GSH-SPCE clearly showed higher sensing signals (peak areas) for each concentration of all the HM ions (Fig. S6(a–c)†) as expected, which was compatible with the fact that GSH offered faster charge-transfer rates with lower charge-transfer resistance, as shown in the cyclic voltammetry (CV) and electrochemical impedance spectroscopy analysis (EIS, Fig. S7 and Table S2†).

3.2.2 Detection of Cd^{2+} under the interference of Pb^{2+} and Cu^{2+}. Cd^{2+} is the most difficult HM to detect compared to Pb^{2+} and Cu^{2+} in their simultaneous presence due to the diminished sensitivity by the presence of the other two, as found in our previous study (Fig. S8†).[27] This could be attributed to three factors in the deposition step: The GSH-SPCE and bare SPCE were tested in 80 ppb Cd^{2+} with different concentrations of Cu^{2+} or Pb^{2+} ranging from 0 to 160 ppb. The Cd signals of the GSH-SPCE only fluctuated slightly with different concentrations of Cu^{2+}, which indicated the minimal influence from Cu^{2+} on the Cd^{2+}-sensing signals (Fig. 3a). Regarding the evaluation of Pb^{2+} interference, the GSH-SPCE enabled observable Cd^{2+} signals, while the counterpart only showed unmeasurable signals (Fig. 3b). This proved that the GSH significantly alleviated the Pb^{2+} interference on Cd^{2+} and allowed the simultaneous detection of both, which is incredibly difficult for bare SPCEs.

To further evaluate the influence of the Pb^{2+} concentration on Cd^{2+} sensitivity, the GSH-SPCE and bare SPCE were used to detect various concentrations of Cd^{2+} in two scenarios: with the presence of 10 ppb and 80 ppb Pb^{2+}. In both scenarios, the GSH was proved to substantially increase the sensitivity of the SPCEs to Cd^{2+}, even though the sensitivity of the GSH-SPCE

could be influenced by the highly concentrated Pb^{2+} ions (Fig. 3c).

In the corresponding voltammograms, intriguingly, the expected Pb peak was divided into two peaks: peak A, centred at −0.56 V and commonly identified as the main Pb peak,[57] and peak B at −0.49 V (Fig. 3(d and e)). However, the splitting of peak B was unobservable when detecting only Pb^{2+} at the same concentration using both electrodes of GSH-SPCE and bare SPCE (Fig. S9†). This suggests that it was impossible for peak B to stem from the interaction of Pb–carbon, Pb–GSH, or Pb–Pb, and therefore, the most plausible rationale is that it was caused by Pb–Cd interactions. As reported in the previous study, the appearance of peak B could be attributed to the heterogeneity of the electrode surface where multiple cations are deposited.[57] A similar phenomenon was found in other studies too.[58,59]

Based on the idea that peak B can act as an indicator to evaluate the interaction of Pb and Cd, the maximum current of peak B was plotted with the corresponding Cd^{2+} concentration in Fig. 3f (red rectangle for GSH-SPCE, black rectangle for bare SPCE). The much lower value of the GSH-SPCE with the independence of the Cd^{2+} concentration proves that GSH could help the SPCE to reduce the mutual interference of Cd–Pb.

After investigating the enhancement of Cd^{2+} sensitivity by GSH with the interference of Pb^{2+} or Cu^{2+} separately, the question was aroused whether GSH could even alleviate the mutual interference amongst the 3 HMs ions (*i.e.* Cd^{2+}, Pb^{2+}, and Cu^{2+}). Hence, a comparative experiment between the GSH-SPCE and bare SPCE was conducted in mixed solutions containing these 3 HMs ions with only one HM varying its concentration but the other two remaining at 80 ppb. In Fig. 3(g–i), it can be seen that the GSH-SPCE significantly increased the Cd^{2+} sensitivity and linearity with the interference of Pb^{2+} and Cu^{2+}, compared to the bare SPCE, which on the other hand showed a negligible sensitivity and linearity (Table S3†). However, regarding the sensitivities of Pb^{2+} and Cu^{2+}, both were minimally influenced by the GSH (Fig. 3(h and i)). It was noticeable that the linearity of the GSH-SPCE to detect Cd^{2+} with the existence of Cu^{2+} and Pb^{2+} was relatively low, which could limit its practical use. To solve this issue, machine learning using other fitting algorithms would be considered in practical use.[60]

3.2.3 Simultaneous detection towards Cd^{2+}, Pb^{2+}, and Cu^{2+}. To further understand the simultaneous sensing performance, the GSH-SPCE was examined in a mixed solution containing multi-HMs of Cd^{2+}, Pb^{2+}, and Cu^{2+} with a fixed ratio of 1 : 1 : 1 (Fig. 4). As a comparison, the bare SPCE was tested under the same conditions. The sensitivity of the GSH-SPCE to Cd^{2+} showed a 6-fold enhancement compared to its counterpart; however, the sensitivities of Pb^{2+} and Cu^{2+} were only slightly increased by 1.5 times (Table S3†). Besides, the bare SPCE had poor linearity to Cd^{2+} (R^2 = 0.84) due to the influence from Pb^{2+} and Cu^{2+}, while the GSH-SPCE's linearity was comparatively much better (R^2 = 0.99). Moreover, the GSH-SPCE had a lower LOD to Cd^{2+} (15 ppb) than the bare
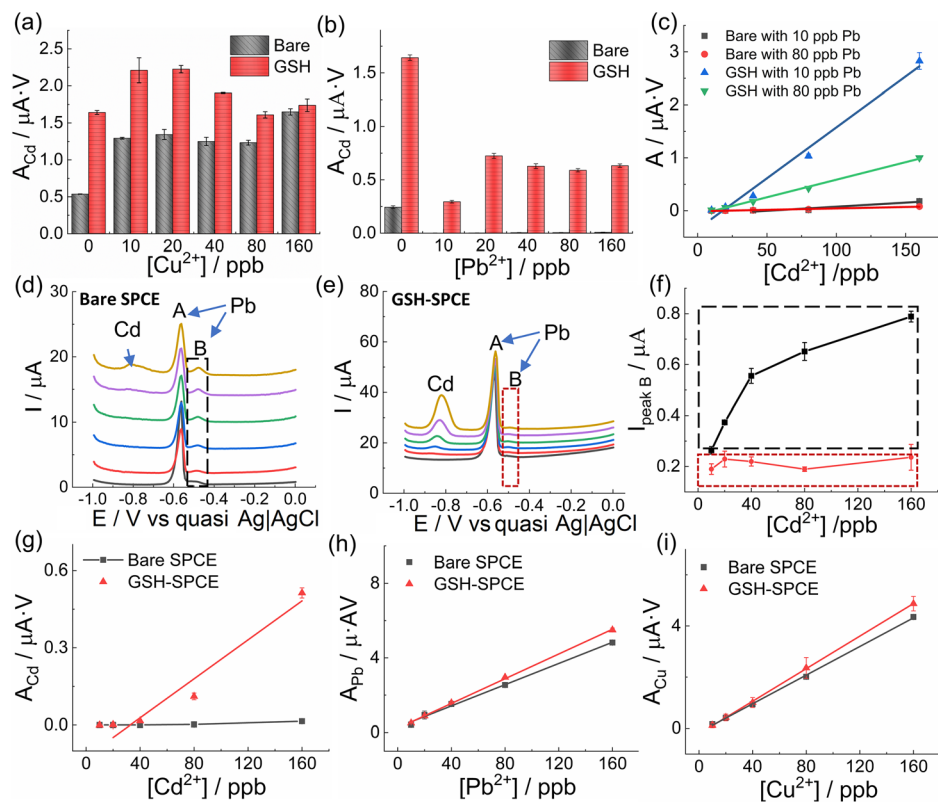
Fig. 3 Sensing performance of the GSH-SPCE and bare SPCE to Cd²⁺ under the mutual interference of Pb²⁺ and Cu²⁺. Peak areas of 80 ppb Cd²⁺ by the GSH-SPCE and bare SPCE with various concentrations of (a) Cu²⁺ and (b) Pb²⁺ respectively. (c) Calibration curves of Cd²⁺ in the GSH-SPCEs and bare SPCEs with Pb²⁺ as an interfering ion at 10 ppb and 80 ppb. Voltammograms of the (d) bare SPCE and (e) GSH-SPCE to detect various concentrations of Cd²⁺ (from 0 (black) to 160 ppb (yellow)) simultaneously with the presence of 80 ppb Pb²⁺. (f) Peak B maxima of the GSH-SPCE (red rectangle) and bare SPCE (black rectangle) with varying the concentration of Cd²⁺. Calibrations of the bare and GSH-SPCEs towards (g) Cd²⁺ under the interference of 80 ppb Pb²⁺ and Cu²⁺, (h) Pb²⁺ under the interference of 80 ppb Cd²⁺ and Cu²⁺, and (i) Cu²⁺ under the interference of 80 ppb Cd²⁺ and Pb²⁺.

SPCE (84 ppb), with a linear range up to 200 ppb. Regarding Cu²⁺ and Pb²⁺, the LODs showed slight improvement by GSH (Table S4†). All the stripping peaks (Fig. 4d) were well separated, where the peaks at −0.86 and −0.2 V referred to Cd and Cu, respectively, and the splitting peaks around −0.5 V could be identified as Pb. The splitting peak could also be attributed to the existence of Cu²⁺ leading to the formation of Cu–Pb intermetallic compounds.[61]

3.2.4 Reusability and reproducibility. The GSH incorporating thiol moieties covalently bound on the graphene sheet was expected to be more robust and reusable than the non-covalently functionalized one. Hence, GSH-SPCE was subjected to 25 continuous measurements in a mixed solution of Cd²⁺, Pb²⁺, and Cu²⁺ ions. The repeatability was recorded as 28.3%, 3.86%, and 6.69% for Cd²⁺, Pb²⁺, and Cu²⁺, respectively. It should be noted that the relatively high repeatability to Cd²⁺ resulted from the highest signals from the first two measurements (Fig. S10a†), which was typical for the bare SPCE, too (Fig. S10b†). Digging out the first two abnormal results, the GSH-SPCE was reused 23 cycling times (RSD ≤ 20%). Compared with other studies in Table S5† demonstrating the reusable times and repeatability, the GSH-SPCEs were found to

be more reusable (23 times) than both the non-covalently functionalized graphene derivatives-modified electrodes (1–10 times) and most bismuth-based electrodes (5–16 times), showing comparable repeatability to Pb²⁺ (3.68%) and Cu²⁺ (6.69%). However, the repeatability of Cd²⁺ was relatively low, which would limit the GSH-SPCE's application in the highly precise detection of Cd²⁺ ions. Instead, low-cost, rapid, and automatic sensing tools (e.g. an automatic in situ sensing boat navigating in large natural waters) that rely on their reusability more than precision could be compatible with the sensing system in this study.[27]

Reproducibility is pivotal for mass production and thus, five GSH-SPCEs and five bare SPCEs were tested in the same mixed solutions of Cd²⁺, Pb²⁺, and Cu²⁺ with the ratio of 1:1:1. All the obtained sensitivities are shown in Table S6.† The reproducibility of GSH-SPCE was 17.5%, 5.1%, and 10.9% to Cd²⁺, Pb²⁺, and Cu²⁺, respectively.

3.2.5 Statical analysis of GSH for enhancing Cd²⁺ sensitivity in simultaneous detection and comparison with other graphene derivatives. To further prove the enhancement by the GSH statistically, Student's t-tests were performed to analyse all the sensitivities data obtained in the reproducibility study
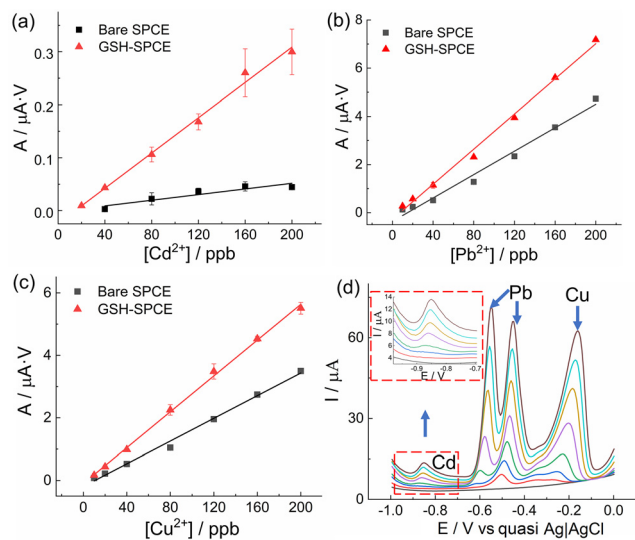
Fig. 4 Sensing performance of the GSH-SPCE and bare SPCE in the simultaneous detection of Cd^{2+}, Pb^{2+}, and Cu^{2+} with varying concentrations (from 0 to 200 ppb) but a fixed ratio of $1:1:1$. Calibration curves of the GSH-SPCE and bare SPCE to (a) Cd^{2+}, (b) Pb^{2+}, and (c) Cu^{2+}. (d) Corresponding voltammograms of GSH-SPCE detecting for a blank sample to 200 ppb mixed solutions (from black to brown).
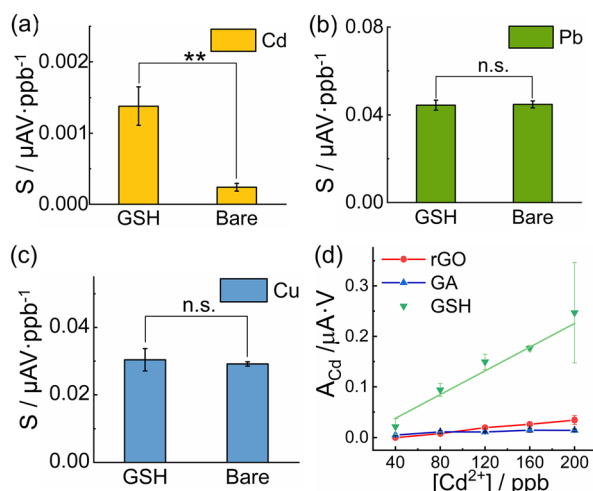

Fig. 5 Reproducibility study and mechanism discussion. The sensitivities to (a) Cd^{2+}, (b) Pb^{2+} and (c) Cu^{2+} of different GSH-SPCEs and different bare SPCEs in reproducibility study. (d) The calibration curves of Cd^{2+} in simultaneous detection using GSH-SPCEs with comparison to other graphene derivatives modified SPCEs.

between the GSH and bare groups (Fig. 5(a–c)). GSH was proven to enhance the sensitivities of the bare SPCEs towards Cd^{2+} statistically at a highly significant level ($p = 0.0005$).[33] Intriguingly, however, the sensitivities to Pb^{2+} and Cu^{2+} did not show any significant difference. This finding corroborated the high specific affinity between GSH and Cd^{2+} amongst these HMs.

To understand whether the selective enhancement of the Cd^{2+} sensitivity originated from the thiol moieties or the gra-

phene sheet in the GSH, we modified SPCEs with other graphene derivatives as references, *i.e.* GA and rGO, with functional groups of –COOH and other oxygen groups, respectively. GA was characterized in our previous study,[41,42] while GO (Angstron Materials, USA) was electrochemically reduced on the SPCE *in situ* after drop casting.[62] However, owing to their different hydrophilicity, the supernatants of GA, GO, and GSH were first adjusted by diluting to secure similar concentrations *via* the Beer–Lambert estimation by UV–Vis ($\sim$0.01 mg ml^{-1}, Fig. S11†), and were then pipetted on to cleaned bare SPCEs with the same optimized procedure.

The GSH showed the best sensitivity to Cd^{2+} compared to GA and rGO (after *in situ* reduction) in the simultaneous detection towards Cd^{2+}, Pb^{2+}, and Cu^{2+} ions (Fig. 5d). This indicated that the bound thiol moieties should be reasonable for their high binding affinity towards Cd^{2+}.

Pearson's hard and soft acid and base (HSAB) theory can elucidate the phenomenon whereby soft bases (*e.g.* RSH), rather than hard bases (*e.g.* RCOOH), have a stronger affinity for soft acids (*e.g.* Cd^{2+}).[63] *Vice versa*, compared to Pb^{2+} and Cu^{2+} as intermediate acids,[64] Cd^{2+} as a soft acid presented a better affinity to soft bases, like thiols. Typical examples are summarized in Table S7.† Therefore, the free thiol groups in the GSH provided potent coordination sites for Cd^{2+} during the deposition step and thus, increased the concentration of Cd^{2+} on the electrode surface, even under the interference of Pb^{2+} and Cu^{2+}, which resulted in the selective enhancement of the Cd^{2+} sensitivity.

Moreover, the defects in the GSH nanosheets structures (as can be seen in the relatively high I_D/I_G in Fig. S2†) could provide active binding sites for HM ions on the graphene backbones, which could reduce the ions' competition and facilitate the deposition of Cd^{2+} on the working electrode.[65]

3.3 Interference study of GSH-SPCE and its validation with real samples

To mimic real samples, the interference of other ions (*i.e.* Na$^+$, K$^+$, Ca^{2+}, Mg^{2+}, Ni^{2+}, Zn^{2+}, As^{3+} and Hg^{2+} with the 5-fold concentration of Cd^{2+}, Pb^{2+}, and Cu^{2+}) was studied using the GSH-SPCE. The responses of Cd^{2+}, Pb^{2+}, and Cu^{2+} decreased to 74%, 97%, and 89%, respectively, compared to those without interference (Fig. S12†). The signal loss of Cd^{2+} could be caused by Hg^{2+}, which is also a soft acid competing for the thiol active sites.

GSH-SPCE was then validated with tap water with spiked HMs (Cd : Pb : Cu = 1 : 1 : 1) from 10 ppb to 200 ppb (Fig. S13†). The obtained sensitivity values of Cd^{2+}, Pb^{2+}, and Cu^{2+} were close to the values in the standard solutions (Table S3†). Afterwards, a recovery/accuracy test was conducted using the GSH-SPCE in spiked tap water containing 90 ppb of Cd^{2+}, Cu^{2+}, and Pb^{2+}. All the recoveries were above 80% as shown in Table S8,† where the reference data from ICP-MS is also shown. Integrating filtration membranes or adding mask reagents in the fluidic sensing system could further improve the accuracy of untreated real samples from a practical point

of view. Modifying the anti-fouling materials on electrodes could be another option and needs to be solved in the future.

3.4 Comparison with other reported studies

Last, the GSH-SPCE was compared to other studies, as shown in Table S9.† Although the LODs of the GSH-SPCE (15, 11, and 6 ppb for Cd^{2+}, Pb^{2+}, and Cu^{2+}, respectively) were not as low as those of the GCEs (sub-ppb) and some bismuth-based SPCEs, there are several advantages of the GSH-SPCE to note.

First, the metal-free GSH-SPCE is considerably more sustainable and economical to depress mutual interferences. Unlike the traditional strategy, the synthesis of GSH does not involve any metallic precursor and it can be easily prepared in a mass-productive way owing to its wet-chemical synthesis, which matches the large manufacture of SPCEs. Particularly, the graphite fluoride (GF) used in the synthesis of the GSH is a cheap industrial solid lubricant and is easily accessible.

Besides, the covalent bond (between amino groups in cysteamine and carbon atoms on the graphene backbone) gives GSH extremely high stability in the condition of a largely negative potential and highly acidic solution, which is necessary for HM detection. These functionalized moieties could be maintained on GSH without degradation or deformation in the continuous cycling measurements. The reusable cycle (23 times) surpassed other studies using non-covalently functionalized graphene (1–10 times) and most bismuth-modified SPCEs (5–16 times, Table S5†).

Additionally, our testing system could perform *in situ* and automatic measurements, allowing the scenario of monitoring drinking water quality at home. In the future, SPCEs modified with various moieties could be achieved *via* our approach utilizing the covalent interaction between the amines of versatile molecules and FG. New graphene derivatives with specific moieties can be designed and synthesized according to their binding affinity to certain HM pollutants to reduce mutual interference.

Conclusion

Sustainable GSH (graphene covalently functionalized with free thiol groups) was synthesized and modified on SPCEs in order to alleviate mutual interference. GSH was proven to be able to boost the diminished sensitivity of the SPCE to Cd^{2+} from Pb^{2+} and Cu^{2+}. The Cd^{2+} sensitivities of GSH-SPCEs demonstrated a significant difference from those of bare SPCEs, while the sensitivities to Pb^{2+} and Cu^{2+} were not influenced. The selective enhancement to Cd^{2+} originated from the free thiol groups in the GSH, according to the best Cd^{2+} sensitivity in the comparative tests of GA and rGO. This phenomenon can be explained by the HSAB theory, whereby the thiol (soft base) had a good affinity to Cd^{2+} (soft acid). In multi-HMs simultaneous detection, the GSH-SPCE could detect Cd^{2+}, Pb^{2+}, and Cu^{2+} at up to 15, 11, and 6 ppb, respectively. The high reusability (23 times), owing to the covalent functionalization mode, outperforms the state-of-the-art SPCEs based on non-covalent functionalization

routes, with a comparative repeatability of Pb^{2+} and Cu^{2+}, even though the relatively low repeatability of Cd^{2+} could limit their practical use in highly precise detection. Last, the *in situ* and automatic testing system, including the reusable GSH-SPCE, was validated with spiked tap water. Importantly, unlike conventional strategies involving metallic additives that can cause secondary pollution and have limited reusability, our approach offers a metal-free and robust sensing platform. Versatile functionalization with other chemical groups can be designed to construct selective electrodes to target certain analytes in the future.

Author contributions

Q. Y.: conceptualization, methodology, investigation, data curation, visualization, writing–original draft preparation, and writing–review & editing; E. P. N.: conceptualization, methodology, investigation, supervision, writing–original draft preparation, and writing–review & editing; D. P.: methodology, investigation, visualization, and writing–review & editing; V. Š.: methodology, investigation, visualization, and writing–review & editing; V. H.: methodology, investigation, visualization, and writing–review & editing; G. R.: investigation and writing–review & editing; C. C. C. S: investigation and writing–review & editing; A. B.: supervision and writing–review & editing; M. O.: supervision and writing–review & editing; A. M.: conceptualization, supervision and writing–review & editing.

Conflicts of interest

There are no conflicts to declare.

Acknowledgements

References

1 M. Csuros, *Environmental Sampling and Analysis for Technicians*, CRC Press, 1st edn, 1994.

2 G. Aragay, J. Pons and A. Merkoçi, *Chem. Rev.*, 2011, **111**, 3433–3458.

3 List of chemicals for Water Framework Directive assessments, https://www.gov.uk/government/publications/list-of-chemicals-for-water-framework-directive-assessments.

4 R. P. Schwarzenbach, B. I. Escher, K. Fenner, T. B. Hofstetter, C. A. Johnson, U. von Gunten and B. Wehrli, *Science*, 2006, **313**, 1072–1077.

5 K. Jomova and M. Valko, *Toxicology*, 2011, **283**, 65–87.

6 J. G. Osteryoung and R. A. Osteryoung, *Anal. Chem.*, 1985, **57**, 1–6.

7 V. Mirceski, S. Skrzypek and L. Stojanov, *ChemTexts*, 2018, **4**, 1–14.

8 K. Xu, P. Clara, A. Marchoud and A. Crespo, *Chemosensors*, 2021, **9**, 107.

9 K. C. Honeychurch and J. P. Hart, *TrAC, Trends Anal. Chem.*, 2003, **22**, 456–469.

10 M. Cadevall, J. Ros and A. Merkoçi, *Electrophoresis*, 2015, **36**, 1872–1879.

11 A. J. Borrill, N. E. Reily and J. V. Macpherson, *Analyst*, 2019, **144**, 6834–6849.

12 C. Huangfu, L. Fu, Y. Li, X. Li, H. Du and J. Ye, *Electroanalysis*, 2013, **25**, 2238–2243.

13 S. Xiong, B. Yang, D. Cai, G. Qiu and Z. Wu, *Electrochim. Acta*, 2015, **185**, 52–61.

14 Y. Wei, R. Yang, X. Chen, L. Wang, J. H. Liu and X. J. Huang, *Anal. Chim. Acta*, 2012, **755**, 54–61.

15 K. E. Toghill, L. Xiao, G. G. Wildgoose and R. G. Compton, *Electroanalysis*, 2009, **21**, 1113–1118.

16 Y. Li, G. Sun, Y. Zhang, C. Ge, N. Bao and Y. Wang, *Microchim. Acta*, 2014, **181**, 751–757.

17 C. M. Willemse, K. Tlhomelang, N. Jahed, P. G. Baker and E. I. Iwuoha, *Sensors*, 2011, **11**, 3970–3987.

18 P. M. Lee, Z. Chen, L. Li and E. Liu, *Electrochim. Acta*, 2015, **174**, 207–214.

19 A. F. Al-Hossainy, A. A. I. Abd-Elmageed and A. T. A. Ibrahim, *Arabian J. Chem.*, 2019, **12**, 2853–2863.

20 J. Zheng, M. A. Rahim, J. Tang, F.-M. Allioux and K. Kalantar-Zadeh, *Adv. Mater. Technol.*, 2022, **7**, 2100760.

21 *CRC Handbook of Chemistry and Physics*, 97th edn, pp. 14–17.

22 R. Mohan, *Nat. Chem.*, 2010, **2**, 336.

23 L. J. Stephens, S. Munuganti, R. N. Duffin, M. V. Werrett and P. C. Andrews, *Inorg. Chem.*, 2020, **59**, 3494–3508.

24 J.-H. Hwang, X. Wang, D. Zhao, M. M. Rex, H. J. Cho and W. H. Lee, *Electrochim. Acta*, 2019, **298**, 440–448.

25 S. B. Hočevar, I. Švancara, K. Vytřas and B. Ogorevc, *Electrochim. Acta*, 2005, **51**, 706–710.

26 P. K. Sahoo, B. Panigrahy, S. Sahoo, A. K. Satpati, D. Li and D. Bahadur, *Biosens. Bioelectron.*, 2013, **43**, 293–296.

27 Q. Yang, B. Nagar, R. Alvarez-Diduk, M. Balsells, A. Farinelli, D. Bloisi, L. Proia, C. Espinosa, M. Ordeix, T. Knutz, E. De Vito-Francesco, R. Allabashi and A. Merkoçi, *ACS ES&T Water*, 2021, **1**, 2459–2555.

28 X. Zhu, B. Liu, H. Hou, Z. Huang, K. M. Zeinu, L. Huang, X. Yuan, D. Guo, J. Hu and J. Yang, *Electrochim. Acta*, 2017, **248**, 46–57.

29 Y. Chu, F. Gao, F. Gao and Q. Wang, *J. Electroanal. Chem.*, 2019, **835**, 293–300.

30 Z. Y. Song, X. Y. Xiao, S. H. Chen, Y. Li, Y. F. Yang, C. C. Huang, W. Duan, M. Yang, P. H. Li and X. J. Huang, *Anal. Chem.*, 2022, **94**, 6225–6233.

31 W. Y. Zhou, S. S. Li, J. Y. Song, M. Jiang, T. J. Jiang, J. Y. Liu, J. H. Liu and X. J. Huang, *Anal. Chem.*, 2018, **90**, 4328–4337.

32 W. Wu, M. Jia, Z. Wang, W. Zhang, Q. Zhang, G. Liu, Z. Zhang and P. Li, *Microchim. Acta*, 2019, **186**, 0–9.

33 S. M. Choi, D. M. Kim, O. S. Jung and Y. B. Shim, *Anal. Chim. Acta*, 2015, **892**, 77–84.

34 M. Malhotra, M. Puglia, A. Kalluri, D. Chowdhury and C. V. Kumar, *Sens. Actuators Rep.*, 2022, 100077.

35 V. Georgakilas, M. Otyepka, A. B. Bourlinos, V. Chandra, N. Kim, K. C. Kemp, P. Hobza, R. Zboril and K. S. Kim, *Chem. Rev.*, 2012, **112**, 6156–6214.

36 A. Béraud, M. Sauvage, C. M. Bazán, M. Tie, A. Bencherif and D. Bouilly, *Analyst*, 2021, **146**, 403–428.

37 Y. Liu, J. Zhou, X. Zhang, Z. Liu, X. Wan, J. Tian, T. Wang and Y. Chen, *Carbon*, 2009, **47**, 3113–3121.

38 S. Gilje, S. Dubin, A. Badakhshan, J. Farrar, S. A. Danczyk and R. B. Kaner, *Adv. Mater.*, 2010, **22**, 419–423.

39 D. Matochová, M. Medveď, A. Bakandritsos, T. Steklý, R. Zbořil and M. Otyepka, *J. Phys. Chem. Lett.*, 2018, **9**, 3580–3585.

40 M. Medveď, G. Zoppellaro, J. Ugolotti, D. Matochová, P. Lazar, T. Pospíšil, A. Bakandritsos, J. Tuček, R. Zbořil and M. Otyepka, *Nanoscale*, 2018, **10**, 4696–4707.

41 A. Bakandritsos, M. Pykal, P. Boński, P. Jakubec, D. D. Chronopoulos, K. Poláková, V. Georgakilas, K. Čépe, O. Tomanec, V. Ranc, A. B. Bourlinos, R. Zbořil and M. Otyepka, *ACS Nano*, 2017, **11**, 2982–2991.

42 V. Šedajová, P. Jakubec, A. Bakandritsos, V. Ranc and M. Otyepka, *Nanomaterials*, 2020, **10**, 1731.

43 J. M. R. Flauzino, E. P. Nguyen, Q. Yang, G. Rosati, D. Panáček, A. G. Brito-Madurro, J. M. Madurro, A. Bakandritsos, M. Otyepka and A. Merkoçi, *Biosens. Bioelectron.*, 2022, **195**, 113628.

44 A. Bakandritsos, R. G. Kadam, P. Kumar, G. Zoppellaro, M. Medveď, J. Tuček, T. Montini, O. Tomanec, P. Andrýsková, B. Drahoš, R. S. Varma, M. Otyepka, M. B. Gawande, P. Fornasiero and R. Zbořil, *Adv. Mater.*, 2019, **31**, 1900323.

45 W. A. Henderson and C. J. Schultz, *J. Org. Chem.*, 1962, **27**, 4643–4646.

46 J. Shang, F. Xue and E. Ding, *Chem. Commun.*, 2015, **51**, 15811–15814.

47 C. Pérez-Ràfols, N. Serrano, J. M. Díaz-Cruz, C. Ariño and M. Esteban, *Talanta*, 2016, **155**, 8–13.

48 M. Abdulla, A. Ali, R. Jamal, T. Bakri, W. Wu and T. Abdiryim, *Polymers*, 2019, **11**, 1–19.

49 D. D. Chronopoulos, A. Bakandritsos, M. Pykal, R. Zbořil and M. Otyepka, *Appl. Mater. Today*, 2017, **9**, 60–70.

50 E. C. Vermisoglou, P. Jakubec, A. Bakandritsos, V. Kupka, M. Pykal, V. Šedajová, J. Vlček, O. Tomanec, M. Scheibe, R. Zbořil and M. Otyepka, *ChemSusChem*, 2021, **14**, 3904–3914.

51 I. Tantis, A. Bakandritsos, D. Zaoralová, M. Medveď, P. Jakubec, J. Havláková, R. Zbořil and M. Otyepka, *Adv. Funct. Mater.*, 2021, **31**, 2101326.

52 S. Zhang, *Front. Energy Res.*, 2013, **1**, 10.

53 A. Mishra and B. Jha, *Bioresour. Technol.*, 2009, **100**, 3382–3386.

54 M. Ahn, R. Liu, C. Lee and W. Lee, *J. Nanomater.*, 2019, **2019**, 6464713.

55 A. Ulman, M. Ioffe, F. Patolsky, E. Haas and D. Reuvenov, *J. Nanobiotechnol.*, 2011, **9**, 26.

56 D. Zaoralová, V. Hrubý, V. Šedajová, R. Mach, V. Kupka, J. Ugolotti, A. Bakandritsos, M. Medveď and M. Otyepka, *ACS Sustainable Chem. Eng.*, 2020, **8**, 4764–4772.

57 K. C. Honeychurch, J. P. Hart and D. C. Cowell, *Electroanalysis*, 2000, **12**, 171–177.

58 L. Moreno-Baron, A. Merkoçi and S. Alegret, *Electrochim. Acta*, 2003, **48**, 2599–2605.

59 M. Hadi, A. Rouhollahi and M. Yousefi, *J. Appl. Electrochem.*, 2012, **42**, 179–187.

60 N. Liu, G. Zhao and G. Liu, *J. Electroanal. Chem.*, 2021, **889**, 115227.

61 D. Pan, Y. Wang, Z. Chen, T. Lou and W. Qin, *Anal. Chem.*, 2009, **81**, 5088–5094.

62 J. Kudr, L. Zhao, E. P. Nguyen, H. Arola, T. K. Nevanen, V. Adam, O. Zitka and A. Merkoçi, *Biosens. Bioelectron.*, 2020, **156**, 112109.

63 T. L. Ho, *Chem. Rev.*, 1975, **75**, 1–20.

64 G. Bjørklund, G. Crisponi, V. M. Nurchi, R. Cappai, A. B. Djordjevic and J. Aaseth, *Molecules*, 2019, **24**, 1–32.

65 A. Ambrosi, C. K. Chua, A. Bonanni and M. Pumera, *Chem. Rev.*, 2014, **114**, 7150–7188.